




Pseudomonas aeruginosa Interstrain Dynamics and Selection of Hyperbiofilm Mutants during a Chronic Infection

Erin S. Gloag,^a Christopher W. Marshall,^{b,c} Daniel Snyder,^{b,c} Gina R. Lewin,^{d,e} Jacob S. Harris,^a Alfonso Santos-Lopez,^{b,c} Sarah B. Chaney,^a Marvin Whiteley,^{d,e}  Vaughn S. Cooper,^{b,c} Daniel J. Wozniak^{a,f}

^aDepartment of Microbial Infection and Immunity, The Ohio State University, Columbus, Ohio, USA

^bDepartment of Microbiology and Molecular Genetics, University of Pittsburgh School of Medicine, Pittsburgh, Pennsylvania, USA

^cCenter for Evolutionary Biology and Medicine, University of Pittsburgh School of Medicine, Pittsburgh, Pennsylvania, USA

^dSchool of Biological Sciences, Georgia Institute of Technology, Atlanta, Georgia, USA

^eEmory-Children's Cystic Fibrosis Center, Atlanta, Georgia, USA

^fDepartment of Microbiology, The Ohio State University, Columbus, Ohio, USA

ABSTRACT Opportunistic pathogens establishing new infections experience strong selection to adapt, often favoring mutants that persist. Capturing this initial dynamic is critical for identifying the first adaptations that drive pathogenesis. Here we used a porcine full-thickness burn wound model of chronic infection to study the evolutionary dynamics of diverse *Pseudomonas aeruginosa* infections. Wounds were infected with a mixed community of six *P. aeruginosa* strains, including the model PA14 strain (PA14-1), and biopsies taken at 3, 14, and 28 days postinfection. Hyperbiofilm-forming rugose small-colony variants (RSCVs) were the earliest and predominant phenotypic variant. These variants were detected on day 3 and persisted, with the majority evolved from PA14-1. Whole-genome sequencing of PA14-1 RSCV isolates revealed driver mutations exclusively in the *wsp* pathway, conferring hyperbiofilm phenotypes. Several of the *wsp* mutant RSCVs also acquired CRISPR-Cas adaptive immunity to prophages isolated from the *P. aeruginosa* wound isolate (B23-2) that was also present in the inoculum. These observations emphasize the importance of interstrain dynamics and the role of lysogenic phages in the survival of an invading pathogen. Rather than being a side effect of chronicity, the rapid rise of RSCVs in wounds is evidence of positive selection on the Wsp chemosensory system to produce mutants with elevated biofilm formation capacity. We predict that RSCVs provide a level of phenotypic diversity to the infecting bacterial community and are common, early adaptations during infections. This would likely have significant consequences for clinical outcomes.

IMPORTANCE Bacteria adapt to infections by evolving variants that are more fit and persistent. These recalcitrant variants are typically observed in chronic infections. However, it is unclear when and why these variants evolve. To address these questions, we used a porcine chronic wound model to study the evolutionary dynamics of *Pseudomonas aeruginosa* in a mixed-strain infection. We isolated hyperbiofilm variants that persisted early in the infection. Interstrain interactions were also observed, where adapted variants acquired CRISPR-mediated immunity to phages. We show that when initiating infection, *P. aeruginosa* experiences strong positive selection for hyperbiofilm phenotypes produced by mutants of a single chemosensory system, the *Wsp* pathway. We predict that hyperbiofilm variants are early adaptations to infection and that interstrain interactions may influence bacterial burden and infection outcomes.

KEYWORDS CRISPR-Cas, *Pseudomonas aeruginosa*, RSCV, *Wsp*, bacteriophages, biofilms, chronic infection, cyclic di-GMP, evolution, exopolysaccharide

Citation Gloag ES, Marshall CW, Snyder D, Lewin GR, Harris JS, Santos-Lopez A, Chaney SB, Whiteley M, Cooper VS, Wozniak DJ. 2019.

Pseudomonas aeruginosa interstrain dynamics and selection of hyperbiofilm mutants during a chronic infection. mBio 10:e01698-19. <https://doi.org/10.1128/mBio.01698-19>.

Editor Frederick M. Ausubel, Mass General Hospital

Copyright © 2019 Gloag et al. This is an open-access article distributed under the terms of the [Creative Commons Attribution 4.0 International license](https://creativecommons.org/licenses/by/4.0/).

Address correspondence to Daniel J. Wozniak, Daniel.Wozniak@osumc.edu.

E.S.G. and C.W.M. contributed equally to this work.

This article is a direct contribution from a Fellow of the American Academy of Microbiology. Solicited external reviewers: Stephen Lory, Harvard Medical School; Paul Turner, Yale University.

[The article was updated on 5 September 2019 to correct spacing issues in table 3.]

Received 8 July 2019

Accepted 10 July 2019

Published 13 August 2019

Chronic infections that persist despite extensive treatment are often attributed to biofilms, which are communities of adhered microorganisms encased in an extracellular polymeric substance (EPS) (1). Complicating chronic infections is the high likelihood that bacterial populations adaptively evolve, producing novel subpopulations with persistent phenotypes and increased fitness. When opportunistic pathogens leave an environmental reservoir to colonize a host, there are potentially many beneficial mutations available for selection in this environment. Defining this new fitness landscape and the evolutionary dynamics of pathogen adaptation to the host environment is critical to understanding infection pathology, as the emergence and selection of adapted variants in an infection are often associated with worsening clinical outcomes (2). Adapted variants are typically identified later in the infection, when eradication has become increasingly difficult. By monitoring the rise of adapted genotypes within pathogen populations, as the infection becomes established, we can understand the environment in which the pathogen adapts and predict the fitness constraints as a result of the adaptation. This may enable prediction of evolutionary pathways that could be targeted to improve treatment efficacy (3, 4).

Of interest to chronic infections are the emergence of rugose small-colony variants (RSCVs), which are associated with persistence (5). RSCVs are characterized by high fitness in biofilms, and they have been isolated from chronic infections (6, 7) and *in vitro*-grown biofilm experiments (8, 9). This suggests that there is strong selection for ecological diversification in both *in vivo*- and *in vitro*-grown biofilms. One of the most studied bacterial adaptive responses to chronic infection is that of *Pseudomonas aeruginosa* to the cystic fibrosis (CF) lung (10). CF patients exhibit airway abnormalities, where *P. aeruginosa* biofilms commonly colonize the mucus lining, and establish persistent pulmonary infections (11, 12). RSCVs are isolated from up to 50% of *P. aeruginosa*-positive CF sputum samples (6, 7). When isolated, RSCV frequencies range widely between patient samples, from 0.1 to 100% of the total population (7, 13). However, in comparison to the chronic pulmonary infections of CF patients, little is understood regarding *P. aeruginosa* adaptation in other common chronic infections, such as chronic wounds. Furthermore, understanding the selective forces that drive the emergence and frequency of RSCVs is important because of their association with hyperbiofilm-forming phenotypes (14, 15), increased tolerance to antimicrobials (13), and enhanced resistance to immunity (5).

The RSCV phenotype is commonly caused by mutations in pathways that lead to elevated cyclic diguanylate monophosphate (c-di-GMP) (2). c-di-GMP is a messenger molecule that signals the transition from planktonic to biofilm lifestyle in many bacteria (16). In *P. aeruginosa*, increased c-di-GMP, among many responses, leads to overproduction of exopolysaccharides, Psl and Pel, and matrix proteins (14, 17, 18). RSCVs with driver mutations in the Wsp (wrinkly spreader) pathway, originally identified in *Pseudomonas fluorescens* (19, 20), are commonly isolated from *in vitro*-grown biofilms, where approximately 70% of isolated *P. aeruginosa* RSCVs can be complemented by *wspF* in *trans* (17). Mutations in the Wsp pathway have been implicated in *P. aeruginosa* evolution in CF patients (21, 22). However, their importance in relation to other identified adaptive mutations and frequency in other chronic infections is unclear.

Despite our understanding of the divergent phenotypes of evolved variants, it is currently unclear which mutations and pathways experience selection in an infection, what new niches become occupied, and how these adaptations enable pathogen survival. It is often not feasible to monitor bacterial evolution from the onset of infection, as it is difficult to understand microbial dynamics in a clinical setting due to patient care, sampling difficulties, and cost. This has similarly proven challenging to monitor in a research setting, as there are few chronic infection models that mimic what is observed clinically. Furthermore, mutations also exist in the context of the larger microbial community. Chronic infection models typically address the adaptive traits of only a single founding clone, but susceptible individuals are continually exposed to different strains of opportunistic pathogens, particularly in the case of environmental organisms like *P. aeruginosa*. To address these challenges, we used a

TABLE 1 Strains and plasmids used in this study

Strain or plasmid	Relevant genotype and/or characteristic(s)	Reference or source
<i>P. aeruginosa</i> strains used in the infection ^a		
PA14-1	Barcode CAAAAGGACA; Gent	
PAO1-B11	Barcode GTGTCGTGGG; Gent	
B23-2	Wound isolate; barcode GCCTATTGTG; Gent	Lubbock, TX
CF18-1	Nonmuroid CF isolate; barcode GTTACGTCAA; Gent	60
MSH10-2	Water isolate; barcode TATCAGATTT; Gent	60
S54485-1	UTI ^b isolate; barcode TTAACACTAGG; Gent	60
<i>P. aeruginosa</i> strains		
PA14		
PA14Δ <i>wspF</i>	Clean <i>wspF</i> deletion	
PAO1		
PAO1Δ <i>wspF</i>	Clean <i>wspF</i> deletion (JJH356)	
PA14-1 <i>attB</i> :: <i>lacZ</i>	<i>lacZ</i> from miniCTX- <i>lacZ</i> introduced at the <i>attB</i> site	This study
RSCV-2 <i>wt-wspA</i>	Variant <i>wspA</i> replaced by the wild-type allele	This study
RSCV-1 <i>wt-wspA</i>	Variant <i>wspA</i> replaced by the wild-type allele	This study
RSCV-40 <i>wt-wspA</i>	Variant <i>wspA</i> replaced by the wild-type allele	This study
<i>E. coli</i> strains		
NEB5-α		NEB ^c
S17		NEB
Plasmids		
pEX18Ap	Gene deletion vector	47
pEX18Ap:: <i>wt-wspA</i>	<i>wspA</i> -complementing construct	This study
pCdrA:: <i>gfp</i>	CdrA promoter fused to <i>gfp</i> ; Carb	31
pMH487	Empty vector for pCdrA:: <i>gfp</i> ; Carb	31
pJN2133	PA2133 cloned into pJN105; Gent	32
pHERD20T	Empty vector; Carb	56
pHERD2133	PA2133 from pJN2133 cloned into pHERD20T; Carb	This study
miniCTX- <i>lacZ</i>	Tet	58

^aAll strains used in the infection are resistant to gentamicin. Barcodes are located at the Tn7 site on the genome.

^bUTI, urinary tract infection.

^cNEB, New England Biolabs.

porcine full-thickness thermal injury wound model, which closely reflects human clinical chronic wounds (23–27), and is considered a general model for studying chronic infections established by bacterial biofilms (23, 25–27). Here, these wounds were inoculated with a coinfection of six *P. aeruginosa* strains, and we determine which strains persist, which produce adaptive colony variants, and identify the genetic and physiological pathways of adaptive evolution.

RESULTS

***P. aeruginosa* strains PA14-1 and PAO1-B11 were predominant in a mixed-strain chronic burn wound infection.** To determine the relative fitness of different *P. aeruginosa* strains and how the population evolves during chronic infection, we infected porcine full-thickness burn wounds with an inoculum consisting of approximately equal (but not identical) numbers of six different *P. aeruginosa* strains. Wounds were infected with two model strains (PA14-1 and PAO1-B11), three clinical isolates (B23-2, CF18-1, and S54485-1), and a water isolate (MSH10-2) (Table 1). Each strain had a unique nucleotide barcode introduced at the neutral Tn7 site (Table 1). These strains share similar growth kinetics (see Fig. S1A and B in the supplemental material) and biofilm formation capacity (Fig. S1C). Wound biopsies were taken 3, 14, and 28 days postinfection (dpi) for bacterial quantification.

Colony-forming unit (CFU) counts revealed that wounds remained colonized with approximately 10⁵ bacteria up to 28 dpi (Fig. 1A). To quantify the proportion of each strain over time, genomic DNA was isolated from biopsy tissue samples, and amplicons spanning the barcode were sequenced. As early as 3 dpi, PA14-1 and PAO1-B11 became the predominant strains in the infection, outcompeting the four other strains

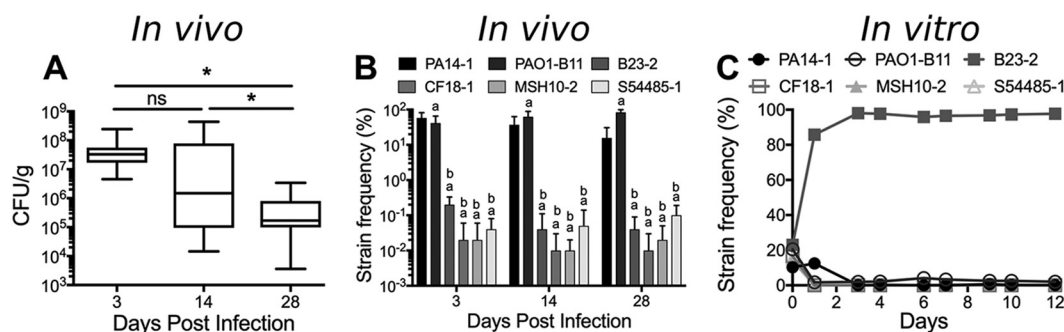


FIG 1 *P. aeruginosa* burden in a mixed-strain chronic burn wound infection. (A) Biopsies were taken from wounds at 3, 14, and 28 dpi. Biopsy specimens were homogenized and plated for CFU/gram, each plated in triplicate, with a minimum of four biopsy specimens taken from each wound. Significance was determined using a one-way ANOVA. ns, not significant; *, *P* value of <0.05. (B) Genomic DNA was isolated from homogenized tissue, and the strain-specific barcodes at the Tn7 site were sequenced. A minimum of four biopsy specimens from each wound was sequenced. Significance was determined using a one-way ANOVA: a, *P* value of <0.05 compared to PA14-1; b, *P* value of <0.05 compared to PAO1-B11. (C) The six ancestor strains were competed in planktonic culture *in vitro* for 12 days. Three replicates were performed at each time point. For panels B and C, the proportion of strain barcodes were expressed as a percentage of the total sequence reads to determine the relative frequency of each strain.

by orders of magnitude (Fig. 1B). To test whether PA14-1 and PAO1-B11 dominated in the infection due to host factors or due to interstrain competition, the six ancestor strains were competed together in planktonic culture *in vitro*, at similar starting frequencies used to inoculate the porcine wounds. Under these conditions, after 24 h, the wound isolate B23-2 outcompeted the other five strains (Fig. 1C). After 3 days, B23-2 remained the predominant strain, with PAO1-B11 the only other strain to be consistently detected, at approximately 2% of the population (Fig. 1C). This indicates that the predominance of PA14-1 and PAO1-B11 in the wounds was likely due to *in vivo*-specific factors (see Discussion).

RSCVs were selected for during porcine chronic burn wound infections. To identify functionally distinct mutants within the infections, we used colony morphology as an indicator (28, 29). Homogenized biopsy specimens were grown on Vogel-Bonner minimal medium supplemented with Congo red and brilliant blue dyes (VBMM). RSCVs were isolated from all three time points, with two subpopulations observed; one that had a pink, rugose phenotype and a second that had an orange, textured phenotype (Fig. 2A). The RSCV phenotype was stable across four passages on selective and nonselective growth media, consistent with the hypothesis that these variants were due to stable genetic mutations. In comparison, RSCVs were not isolated from the *in vitro* planktonic competition.

The total RSCV abundance in the wounds was quantified as a percentage of the total *P. aeruginosa* burden. RSCV frequency was low 3 dpi ($0.02\% \pm 0.12\%$), peaked at 14 dpi, at approximately 2% ($2.15\% \pm 5.25\%$), and declined at 28 dpi ($0.19\% \pm 0.65\%$) (Fig. 2B). Despite their low prevalence, their rapid rise to detectable frequency allowed us to quantify the selective pressure acting on RSCVs in the wound, across a range of possible starting frequencies, according to equation 1. The selective coefficient (*s*) was >0.1, demonstrating that RSCVs were under strong positive selection (Table 2).

RSCVs were detected only from the model strains PA14-1 (the pink phenotype [Fig. 2A]) and PAO1-B11 (the orange phenotype [Fig. 2A]). RSCVs derived from PA14-1 were isolated across all time points, whereas PAO1-B11 RSCVs were isolated from 14 and 28 dpi. At the later two time points, PA14-1 RSCVs remained the predominant subpopulation (Fig. 2C).

PA14-1 RSCVs contained driver mutations exclusively within the *wsp* pathway. As PA14-1 RSCVs were the predominant evolved phenotype, we focused on this subpopulation for the remainder of this study. Whole-genome sequencing was performed on 27 randomly selected PA14-1 RSCVs to identify the mutation(s) accounting for the RSCV phenotype.

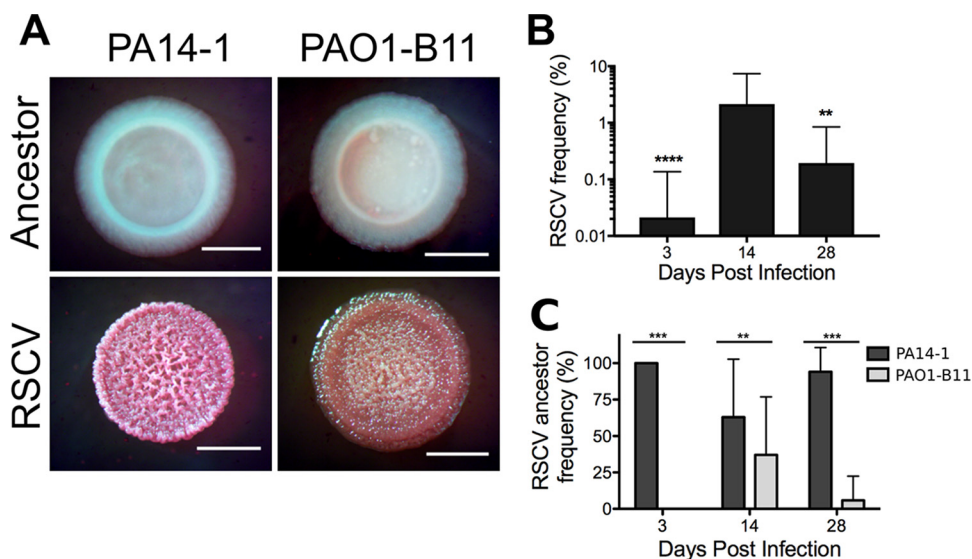


FIG 2 *P. aeruginosa* RSCVs isolated from porcine chronic burn wound infections. (A) Representative colony morphologies of RSCVs isolated from homogenized porcine burn wound tissue. RSCVs were plated on VBMM, and the colony morphology was compared to the ancestor strain (labeled). Bars, 2 mm. (B) Frequency of the total RSCV population isolated at each time point expressed as a percentage of the total *P. aeruginosa* population. Data are presented as mean \pm standard deviation (SD). Significance was determined using a one-way ANOVA: **, *P* value of <0.01; ****, *P* value of <0.0001 compared to 14 dpi. (C) Frequency of the ancestor strain that the RSCVs evolved from, expressed as a percentage of the total RSCV subpopulation. Data presented as mean \pm SD. Significance was determined using a Student's *t* test: **, *P* value of <0.01; ***, *P* value of <0.001.

We identified putative driver mutations exclusively in the *wsp* cluster, specifically, an in-frame, 42-bp deletion ($\Delta 285-298$ aa) in *wspA*, and a frameshift 5-bp deletion (V154fs) in *wspF* (Table 3). RSCVs with the *wspA* mutation were predominant across all time points, and *wspF* mutants were identified only at 14 dpi. Using RSCV-2 as a representative *wspA* mutant, we replaced the variant *wspA* with the wild-type allele using two-step allelic recombination to rescue the deletion. This resulted in the RSCV colony phenotype reverting to the wild-type phenotype (Fig. 3), demonstrating that the *wspA* $\Delta 285-298$ mutation was responsible for the RSCV phenotype.

Some of the RSCVs also possessed secondary mutations (Table 3), possibly demonstrating further adaptation in the wound. Two *wspA* RSCVs from 3 dpi (Table 3; RSCV-1 and RSCV-4) underwent a 14,299-bp deletion that removed the remaining *psl* operon. PA14 naturally lacks *Psl*, since *pslA-pslD* are absent (30). In these two isolates, the remaining genes of the *psl* operon, *pslE-pslO* were deleted. In the RSCV-1 background, complementation of *wspA* reverted the RSCV colony phenotype to wild type (Fig. 3), indicating that deletion of the remaining *psl* operon did not influence the RSCV phenotype.

Evidence of additional adaptive mutations in the *wsp* cluster was detected on 28 dpi. RSCV-40, in addition to having the *wspA* $\Delta 285-298$ driver mutation, had three separate mutations in *wspD* which led to an early stop codon. However, as the

TABLE 2 Relative fitness, expressed as selection coefficient (*s*), of RSCVs from porcine burn wounds inferred for potential starting frequencies

Starting frequency (RSCV/ancestor)	<i>s</i> (mean \pm SD) at the following days postinfection:		
	3	14	28
1:10 ⁵	0.585 \pm 0.464	0.441 \pm 0.126	0.18 \pm 0.055
1:10 ⁶	0.618 \pm 0.579	0.565 \pm 0.177	0.229 \pm 0.068
1:10 ⁷	0.651 \pm 0.710	0.689 \pm 0.238	0.278 \pm 0.098
1:10 ⁸	0.684 \pm 0.849	0.813 \pm 0.304	0.327 \pm 0.134

TABLE 3 Mutations identified in PA14-1 RSCVs

Sample			Driver mutation			Secondary mutation	
Day	RSCV no.	Wound no.	Gene	Mutation ^a	Frequency (%)	Gene	Mutation
3	1	1	<i>wspA</i>	285-298del		<i>pslO-pslE</i>	Δ14,299 bp
	2	2	<i>wspA</i>	285-298del			
	4	1	<i>wspA</i>	285-298del		<i>pslO-pslE</i> PA14_13130/PA14_13140 <i>fabI/ppiD</i>	Δ14,299 bp TNN→TGC TTC→TCC
Day 3 summary			<i>wspA</i>	285-298del	100		
14	3	4	<i>wspA</i>	285-298del			
	6	4	<i>wspA</i>	285-298del			
	7	4	<i>wspA</i>	285-298del			
	8	4	<i>wspA</i>	285-298del			
	9	4	<i>wspA</i>	285-298del			
	10	4	<i>wspA</i>	285-298del			
	12	4	<i>wspA</i>	285-298del		CRISPR-Cas1/hp ^b Glutamyl-tRNA reductase <i>fabI/ppiD</i>	+60bp L71L (CTG→TTG) TTC→TCC
	13	1	<i>wspA</i>	285-298del			
	14	4	<i>wspA</i>	285-298del			
	16	4	<i>wspA</i>	285-298del			
	17	4	<i>wspA</i>	285-298del			
	20	4	<i>wspF</i>	V154fs			
	24	1	<i>wspA</i>	285-298del			
	27	1	<i>wspA</i>	285-298del			
	28	2	<i>wspA</i>	285-298del			
	36	3	<i>wspF</i>	V154fs			
	37	3	<i>wspA</i>	285-298del			
38	3	<i>wspF</i>	V154fs		CRISPR-Cas1/hp	+60bp	
86	3	<i>wspA</i>	285-298del				
Day 14 summary			<i>wspA</i>	285-298del	84.2		
			<i>wspF</i>	V154fs	15.8		
28	40	1	<i>wspA</i>	285-298del		<i>wspD</i>	G→TT 585bp CT→AG 588-589bp S197S (TCG→TCA) A248V (GCG→GTG)
	42	3	<i>wspA</i>	285-298del		PA14_54090	
	43	3	<i>wspA</i>	285-298del			
	45	3	<i>wspA</i>	285-298del			
	87	2	<i>wspA</i>	285-298del			
	Day 28 summary			<i>wspA</i>	285-298del	100	

^aDeleted amino acid residues are indicated. del, deletion; fs, frameshift.

^bhp, hypothetical protein.

mutations occurred at the *wspD* 3' end, the WspD N terminus may still be expressed and functional (Table 3). In this isolate, complementation of *wspA* reverted the RSCV colony phenotype to wild type (Fig. 3), indicating that the *wspD* mutations did not influence the RSCV colony phenotype. However, this further points toward the strong selective pressure on the Wsp pathway in the chronic infection.

We were also interested in identifying how the PA14-1 non-RSCV population adapted to the infection and whether this population acquired mutations that did not result in divergent colony phenotypes. When we sequenced randomly selected PA14-1 non-RSCV isolates (23 total), relatively few had acquired chromosomal mutations (see Supplementary Results in Text S1 in the supplemental material; Table S1). These isolates had similar levels of biofilm formation and metabolic kinetics compared to the ancestor strain (see Supplementary Results in Text S1; Fig. S2), suggesting that the emergence of RSCVs was the main source of phenotypic diversification in the wounds.

RSCVs isolated from wounds had elevated intracellular c-di-GMP levels. As all PA14-1 RSCVs acquired driver mutations in the *wsp* cluster, we predicted that both the

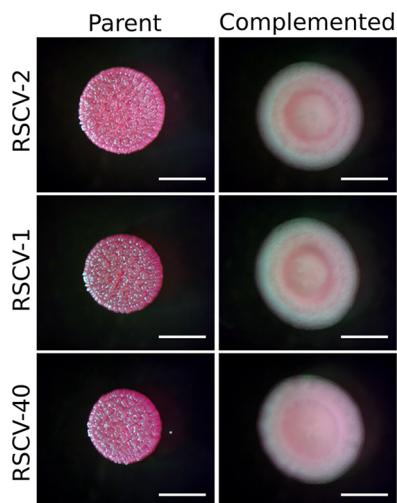


FIG 3 Complementation of the *wspA* $\Delta 285$ -298 mutation. *wspA* was complemented in representative RSCVs by replacing *wspA* $\Delta 285$ -298 with the wild-type allele on the genome. RSCV-2 was selected as a representative RSCV with the *wspA* driver mutation alone. RSCV-1 and RSCV-40 have the *wspA* driver mutation as well as $\Delta pslE$ -*pslO* and *wspD* secondary mutations, respectively. Parent and complemented RSCVs (labeled) were grown on VBMM, and colony morphologies were assessed. Bars, 2 mm.

wspA and *wspF* mutations led to overproduction of c-di-GMP, resulting in the RSCV phenotype. To assess whether c-di-GMP levels were elevated, the pCdrA::*gfp* plasmid (31) was introduced into representative PA14-1 RSCVs. In this plasmid, the *cdrA* promoter, which is under c-di-GMP regulation, is fused to a promoterless *gfp* (31). As expected, the representative PA14-1 RSCVs showed increased levels of green fluorescence compared to the ancestor PA14-1, indicating that the RSCVs had elevated c-di-GMP levels (Fig. 4A). There were no differences in fluorescent signal between the RSCVs, regardless of the driver mutation or the presence of secondary mutations, indicating that the c-di-GMP levels were similar across the representative PA14-1 RSCVs (Fig. 4A). Introduction of a plasmid encoding the phosphodiesterase (PDE; enzyme that degrades c-di-GMP [16]) PA2133, under an arabinose-inducible promoter, into the representative PA14-1 RSCVs reverted the colony morphology to the ancestral type (Fig. 4B). The empty vector did not influence the RSCV colony morphology (Fig. 4B). Collectively, this indicates that elevated c-di-GMP levels were responsible for the RSCV colony phenotype, as has been observed in *P. aeruginosa* *wspF* mutants (32).

Wsp-dependent RSCVs were more fit than the ancestor. RSCV colony morphology and elevated c-di-GMP are often associated with increased biofilm formation capacity. To investigate this possibility, biofilms were grown in microtiter plates for 24 h and stained with crystal violet. All 27 PA14-1 RSCVs displayed increased biofilm formation capacity compared to the ancestor PA14-1 (Fig. 5A). This increased biofilm formation was not due to elevated metabolic activity, as PA14-1 RSCVs had similar growth kinetics, except for an extended lag phase (Fig. S3).

To determine the fitness of PA14-1 RSCVs relative to the ancestor strain *in vitro*, representative RSCVs were grown together with the ancestor PA14-1 tagged with *lacZ* at the neutral *attB* site (PA14-1*attB*::*lacZ*). Strains were grown either in planktonic culture or in a biofilm assay (33). The number of CFUs of each strain and the selection coefficient (*s*) were determined after 2 days as a measurement of fitness. All RSCVs tested were more fit than the ancestor under both modes of growth (Fig. 5B). Fitness in biofilm tended to be greater than in planktonic conditions, but these differences were not significant. The driver mutation did not appear to influence the selection rate, as RSCVs with either the *wspA* $\Delta 285$ -298 or *wspF* V154fs had comparable fitness levels (Fig. 5B; RSCV-2 and RSCV-6 compared to RSCV-20). Furthermore, RSCV-1 ($\Delta pslE$ -*pslO*) had similar fitness levels compared to RSCV-2 and RSCV-6 (Fig. 5B). This suggests that

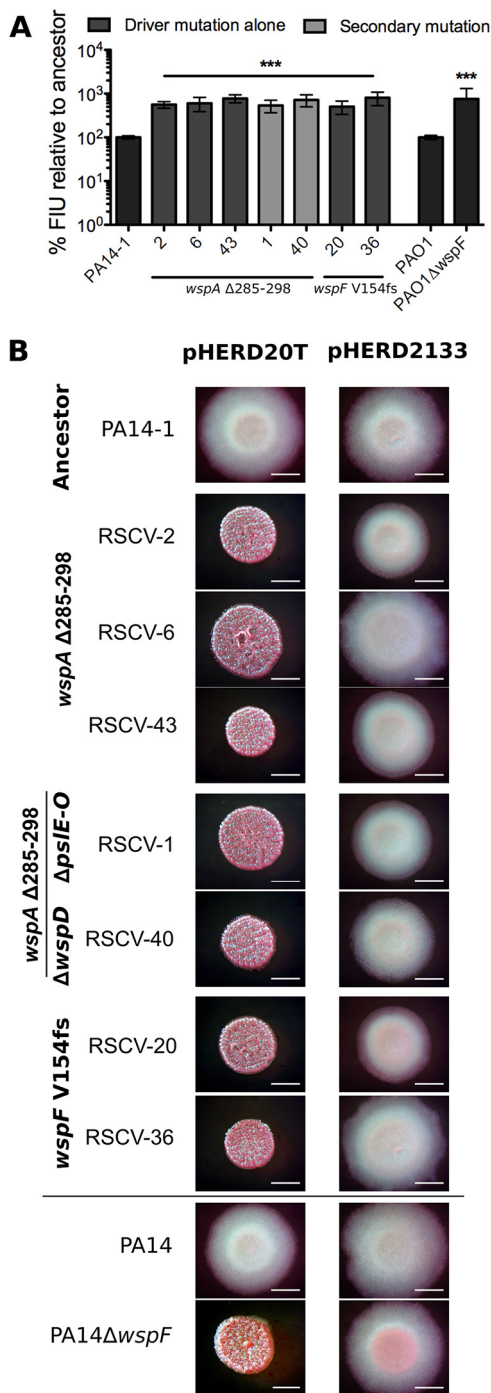


FIG 4 PA14-1 RSCVs have elevated intracellular levels of c-di-GMP which are responsible for the RSCV phenotype. (A) Green fluorescence was measured in representative RSCVs with the c-di-GMP reporter plasmid pCdrA::gfp. Increased GFP signal correlates to increased intracellular c-di-GMP levels. Fluorescence intensity units (FIU) of RSCVs were determined relative to the ancestor strain, which was set at 100%. PAO1Δ*wspF* and its isogenic parent PAO1 were used as controls. Data are presented as mean ± SD (*n* = 3). Significance was determined using a one-way ANOVA: ***, *P* value of <0.001 compared to the ancestor strain. (B) Colony morphology of representative RSCVs grown on VBMM plus 0.1% arabinose. pHERD20T is the empty vector. pHERD2133 has the PDE PA2133 cloned under an arabinose-inducible promoter. PA14Δ*wspF* and its isogenic parent, PA14, were used as controls. For both assays, representative RSCVs were selected. *wspA* mutants from each time point, RSCV-2, RSCV-6, and RSCV-43, were selected. Representative *wspA* mutants with secondary mutations were selected. RSCV-1 has the remaining *psl* operon deleted, and RSCV-40 has the additional *wspD* mutations. Representative *wspF* mutants, RSCV-20 and RSCV-36, were also selected. Bars, 2 mm.

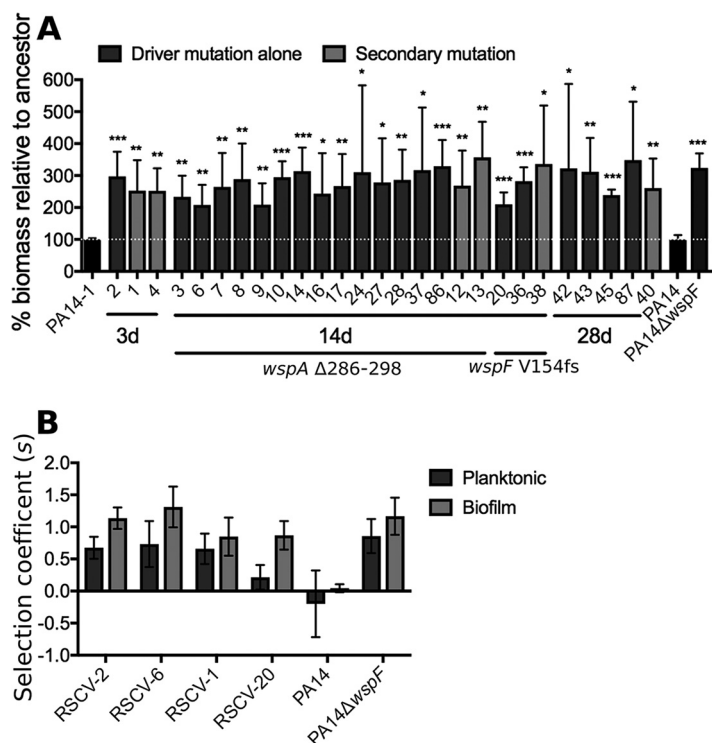


FIG 5 PA14-1 RSCVs have increased biofilm formation and fitness relative to the ancestor PA14-1. (A) PA14-1 RSCVs were grown in 96-well plates for 24 h. Biofilm biomass was stained and quantified by crystal violet. Biofilm biomass levels were expressed as a percentage relative to the ancestor strain, which was set at 100% for each replicate. Data are presented as mean plus SD ($n = 3$). Significance was determined using a one-way ANOVA: *, P value of <0.05 ; **, P value of <0.01 ; ***, P value of <0.001 . (B) Fitness of representative PA14-1 RSCVs relative to the ancestor PA14-1. PA14ΔwspF and its isogenic parent PA14, compared to PA14-1, were used as controls. Strains were grown for 48 h as either a planktonic culture or biofilm, and selection of the RSCVs relative to PA14-1attB::lacZ was determined by calculating the selection rate according to equation 1. Data are presented as mean \pm SD ($n = 5$).

loss of the remaining *psl* operon does not lead to an increased fitness advantage over the RSCV phenotype alone under these laboratory conditions.

***In vivo* acquisition of immunity to viral infection through CRISPR expansion.**

Two of the PA14-1 RSCV isolates, RSCV-12 and RSCV-38, acquired a 60-bp insertion at the clustered regularly interspaced short palindromic repeat (CRISPR)–CRISPR-associated proteins (Cas) locus (Table 3). Both sequences inserted at the intergenic region ($-1549/+271$) between PA14_33350 (RS13600) and PA14_33370 (RS13605) at the genomic position 2,937,205. The last 28 bp of the inserted sequences were identical between the two isolates and aligned to the repetitive elements in the PA14 CRISPR array (CRISPR2 [34]) (Fig. 6A). However, the first 32 bp differed, indicative of CRISPR spacer sequences (Fig. 6A) that are specific to infective mobile genetic elements. A BLAST search of the inserted CRISPR spacer against the ancestor strains aligned to a prophage sequence in the B23-2 genome assembly, indicating potential phage infection across strains (see Supplementary Results in Text S1; Fig. S4).

We therefore predicted that RSCV-12 and RSCV-38 would both be resistant to phages isolated from B23-2 due to CRISPR-Cas adaptive immunity. To test this, we grew B23-2 in mitomycin C and harvested the phage-enriched supernatant. *P. aeruginosa* strains were incubated with the phage lysate, and plaque assays were performed. RSCV-12 and RSCV-38 isolates were resistant to phage infection, with no plaques observed for RSCV-38, and only a single plaque in one replicate for RSCV-12 (Fig. 6B). Infection of RSCV-6 and RSCV-36 (CRISPR⁻), which have identical *wsp* driver mutations as RSCV-12 and RSCV-38 (CRISPR⁺), respectively, had similar levels of phage sensitivity compared to the ancestor PA14-1 (Fig. 6B). This indicates that the acquired CRISPR

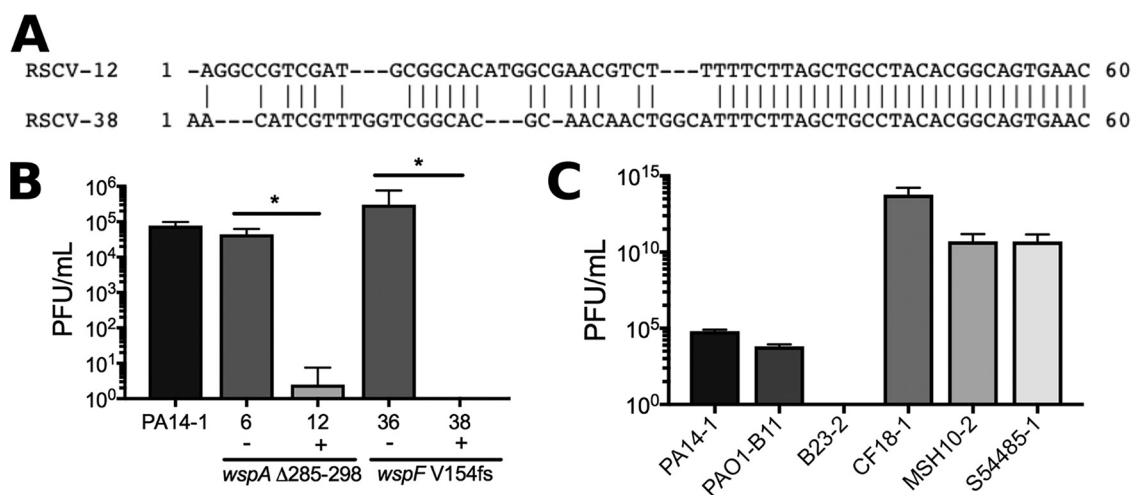


FIG 6 PA14-1 isolates RSCV-12 and RSCV-38 are resistant to infection by phage isolated from B23-2. (A) The 60-bp insertion sequence in the CRISPR array of RSCV-12 and RSCV-38. Prophages were isolated from B23-2, and plaque assays were performed to determine the level of phage infection for representative RSCV isolates (B) and the ancestor *P. aeruginosa* strains (C). RSCV-6 and RSCV-12 both have the same driver *wspA* mutation, while RSCV-36 and RSCV-38 have the same driver *wspF* mutation. The presence (+) or absence (-) of the CRISPR insertion is indicated. The driver mutation for each RSCV is labeled. Data are presented as mean plus SD ($n = 4$). Significance was determined using a Student's *t* test: *, P value of <0.05 .

spacers in RSCV-12 and RSCV-38 produced immunity to phages isolated from B23-2. Each of the ancestor strains was assessed for phage susceptibility, and as expected, B23-2 was resistant to infection, whereas the remaining strains showed various levels of phage sensitivity (CF18-1 > MSH10-2, S54485-1 > PA14-1, PAO1-B11; Fig. 6C).

DISCUSSION

Here we describe the rapid evolution of adaptive *P. aeruginosa* mutants with conspicuous colony phenotypes arising in a clinically relevant model of chronic infection. There is a consensus in the field that evolved variants arise in an infection as a consequence of adaptation over extended periods of time. However, we isolated hyperbiofilm-forming RSCVs from early stages of infection, which suggests that variants may evolve by positive selection more rapidly than originally appreciated. Therefore, contrary to current understanding, RSCVs may be a common, early adaptation during infections, and the selective pressures driving RSCV evolution may persist throughout these infections.

Interestingly, the competitive fitness of the six different *P. aeruginosa* strains differed *in vivo* and *in vitro*. In the wounds, both PA14-1 and PAO1-B11 outcompeted the remaining four strains, while in planktonic culture, B23-2 predominated (Fig. 1). This suggests that *in vivo* environmental factors may be responsible for driving the *P. aeruginosa* strain dynamics in the wound. We predict that *in vitro*, the prophage from B23-2 may be induced and responsible for driving strain competition and dynamics in planktonic culture. It would be interesting to explore this further and to determine, if so, why these dynamics might be dampened *in vivo*. This highlights the notion that fitness *in vitro* does not necessarily correlate to fitness *in vivo* and stresses the importance for using appropriate models when studying *in vivo* systems.

Because of their competitive superiority in the wound, RSCVs were recovered only from PA14-1 and PAO1-B11 (Fig. 2C). *P. aeruginosa* RSCVs were highly adaptive in the infection and in laboratory conditions (Table 2 and Fig. 5B). The estimated selection coefficients determined *in vivo* ($s = 0.180$ to 0.813 ; Table 2) were up to five times greater than those identified in the Lenski long-term evolution lines (35), pointing toward the strong positive selection experienced by RSCVs in the wounds. In addition, similar to our results with PA14-1, *Burkholderia cenocepacia* variants containing *wsp* mutations isolated from an *in vitro* biofilm evolution assay had high selection coefficients (36). Together, these results suggest that *wsp* mutants experience significant

positive selection both *in vivo* and *in vitro* and are broadly adaptive across different environments, where the biofilm lifestyle predominates.

Despite these strong selection coefficients, RSCVs remained at relatively low frequencies throughout the infection (Fig. 2B). This implies that RSCVs may be highly favorable when rare in the wounds, but less favorable when abundant, a process referred to as negative frequency-dependent selection. Negative frequency-dependent selection has been observed for evolved rugose variants of *P. fluorescens* (37–39). Niche competition (37, 38) and division of labor (39) with the ancestor strain drove the evolution of *P. fluorescens* rugose variants from static planktonic and colony growth, respectively. In both cases, diversification of the population was maintained by negative frequency-dependent selection (37–39). In the wound infections, the low-frequency RSCVs could facilitate the ancestor strain in colonizing and establishing biofilms in the wound by producing more EPS. This elevated EPS may enable persistence in an environment constantly exposed to stressors, including fluctuating antibiotics and immune defense (5). However, this may be a shortsighted evolutionary strategy for an opportunistic pathogen, like *P. aeruginosa*, with a significant environmental reservoir. The mutations in *wsp* are rarely reverted and constrain some of the phenotypic plasticity required for survival in fluctuating environments. Accordingly, we predict that in a more homogeneous fitness landscape, RSCVs at low frequencies could be enriched. As an example supporting this hypothesis, higher RSCV frequencies have been observed in CF patients under prolonged exposure to antimicrobials, particularly aerosolized antibiotics (6, 10).

Every sequenced PA14-1 RSCV acquired a driver mutation in the *wsp* cluster, demonstrating that in chronic wounds, the Wsp pathway specifically undergoes selection, and that *wsp* mutants may be more fit than other c-di-GMP-regulating pathways that confer the RSCV phenotype. The *wspA* Δ 285-298 was the most common driver mutation and was isolated early in the infection (Table 3). There are two potential explanations for the rapid rise of this single *wspA* mutant in the infection. The first is that it may have been present in the initial inoculum at undetected levels. The second is that this region may be hypermutable owing to a direct repeat located at either side of the deletion (see Fig. S5A). We are currently unable to discern between these two scenarios; however, it is significant that the population rapidly diversifies in the wound due to strong positive selection of adaptive phenotypes provided by *wsp* mutations.

Supporting the second theory is the observation that mutations in this *wspA* region also appear to be under selection to produce RSCVs in laboratory biofilms (Fig. S5B). The *P. aeruginosa* PAO1 RSCV isolate MJK8, which evolved during biofilm growth in a tube reactor (14), has an in-frame 66-bp deletion (Δ 286–307aa) in the same region as the *wspA* Δ 285-298 isolated here (17). *P. fluorescens* Pfl01, when grown as a colony biofilm, evolved RSCVs with driver mutations in *wspC*, *wspA*, and *wspE* (39). One of the *wspA* mutations was an in-frame 84-bp deletion (Δ 284-311aa), again occurring in the homologous region (39). Finally, *B. cenocepacia* HI2424 RSCVs with *wspA* and *wspE* mutations were isolated from a biofilm bead evolution experiment (36). The majority of mutations identified were nonsynonymous single nucleotide polymorphisms (SNPs); however, one of the *wspA* mutations was an in-frame 21-bp deletion (Δ 307-313aa), again in the homologous region (36) (Fig. S5B). Homology modeling of PA14 WspA suggests that the Δ 285-298 occurs opposite the predicted methylation site (see Supplementary Results in Text S1; Fig. S6). We therefore predict that small deletions in the homologous region could alter how WspA is methylated/demethylated and ultimately lead to constitutive signaling and autoinduction of the Wsp pathway.

In addition to driver mutations, some PA14-1 RSCVs also gained secondary mutations. Of particular interest was the Δ 14,299 bp, which deleted the remaining *psl* operon (Table 3; RSCV-1 and RSCV-4). We predicted that this deletion might lead to increased fitness of the RSCVs, over the RSCV driver mutation alone. However, deletion of the remaining *psl* operon did not provide additional fitness benefits under the conditions tested. Therefore, the remaining *psl* operon (*pslE-pslO*) in PA14 may play a role outside Psl synthesis, which may have a fitness cost in the wound environment.

Additional secondary mutations of interest were the 60-bp insertions in the CRISPR-Cas array of RSCV-12 and RSCV-38 (Table 3 and Fig. 6A), which encoded resistance to phage(s) isolated from B23-2 (Fig. 6B). It has only recently been confirmed that the *P. aeruginosa* type I-F CRISPR-Cas system provides adaptive immunity to phages with a target protospacer (40). This is dependent on the presence of the correct protospacer adjacent motif (PAM) in the mobile genetic element (40). In support of this, both protospacers contain the type I-F CRISPR-Cas-specific GG PAM (Fig. S4). Furthermore, B23-2 contig 107 contained two additional protospacers to which CRISPR spacers in *P. aeruginosa* have been reported (Table S2 and Fig. S4A). Of interest was the observation that PA14 already contains a CRISPR spacer identical to a protospacer in contig 107 (Table S2 and Fig. S4A), possibly indicating that PA14 had already been exposed to the prophage in B23-2. However, the ancestral PA14-1 was still sensitive to infection (Fig. 6B and C), presumably due to the incorrect PAM (Fig. S4A). This highlights the importance of insertion of the correct CRISPR spacer in mediating phage immunity. This is only the second report of CRISPR-Cas acquired immunity in *P. aeruginosa* strains (40), and to our knowledge, this is the first report of CRISPR-Cas adaptive immunity acquired in an infection.

Our data indicate that *P. aeruginosa* experiences strong selective forces in chronic infections, from interstrain phage predation to increased biofilm or aggregate production, and in response rapidly evolve during the initial stages of infection. Parallel evolution of the *wsp* pathway was observed across all time points, suggesting that *wsp* mutants are early, highly beneficial adaptations to infection. This also indicates that the Wsp system is a potent pathway under selection in chronic infections to produce hyperbiofilm variants. This is despite the availability of other c-di-GMP-regulating pathways to produce RSCVs, both *in vivo* and *in vitro* (18, 41–45). We predict that RSCVs produced through the *wsp* pathway may be an adaptation common to chronic infections, and developing therapies that target the RSCV subpopulation or prevent their emergence could be transferrable across these infections.

MATERIALS AND METHODS

Bacterial strains and plasmids. Bacterial strains and plasmids used in this study are detailed in Table 1. Complementation constructs were made using Gibson Assembly (New England Biolabs [NEB]) (46). Primers used to create the constructs are detailed in Table S3 in the supplemental material. Constructs were incorporated into the *P. aeruginosa* genome using two-step allelic recombination as previously described (47).

Porcine full-thickness chronic burn wound model. Swine were housed and studied according to the Ohio State University IACUC-approved protocols. Porcine full-thickness chronic burn wounds were established as previously described (23). Briefly, two pigs were subjected to thermal injury, giving six full-thickness burns per pig and covered with impermeable wound dressings. Wounds were infected 3 days after injury with equal amounts of six different *P. aeruginosa* strains to achieve a final 250- μ l inoculum at 10^8 bacteria (1.6×10^7 each for a total of 1×10^8), which was spread over the wounds and allowed to air dry before the wound dressing was reapplied. Wounds were infected with *P. aeruginosa* strains PA14-1, PAO1-B11, B23-2, CF18-1 (GenBank identifier [ID] [NZ_KI519281](#)), MSH10-2 (GenBank ID [NZ_KE138672](#)), and S54485-1 (GenBank ID [NZ_KI519256](#)). Prior to infection, each strain had been tagged with a unique barcode at the Tn7 site on the genome (see Supplementary Methods in Text S1 in the supplemental material; Table 1).

Wound healing was monitored 3, 14, and 28 days postinfection. At each time point, four to eight 8-mm punch biopsies were taken from two wounds on each pig (four wounds for each time point). Biopsy specimens were homogenized in 1 ml phosphate-buffered saline (PBS) and plated on *Pseudomonas* isolation agar (PIA) supplemented with 100 μ g/ml gentamicin for CFU/gram tissue. To screen for the emergence of adapted *P. aeruginosa* variants, homogenized tissue was also plated onto adjusted Vogel-Bonner minimal medium (VBMM) (see Supplementary Methods in Text S1) supplemented with 100 μ g/ml gentamicin. Colony morphology variants were passaged onto PIA followed by two rounds on Luria agar (LA), before being plated back onto VBMM (without antibiotics) to confirm that the variant phenotype was a result of a stable mutation. Confirmed colony variants were stored at -80°C .

The selection of RSCVs in the wound was determined by calculating the selection coefficient (*s*) according to equation (1) (48)

$$s = \frac{\ln\left(\frac{M_x}{M_0}\right) - \ln\left(\frac{W_x}{W_0}\right)}{T_x} \quad (1)$$

where T_x is day *x* and *M* and *W* are the number of mutant and wild-type cells, respectively, at day *x* and 0.

Sequencing and analysis. To determine the frequency of each strain across the infection, strain-specific barcodes were amplified and given Illumina sequencing adapters as detailed in Supplementary Methods in Text S1. Library sequencing pools were sequenced on NextSeq and MiniSeq High Output SE75 runs at the Petit Institute Molecular Evolution Core Facility at Georgia Institute of Technology. Analysis script is available on GitHub (https://github.com/glew8/Barcode_Sequencing). Briefly, FastQC 0.11.7 and MultiQC v1.5 were used to confirm sufficient sequencing quality (49, 50). Cutadapt 1.13 was used to select sequences with the insert sequence and parse reads containing each barcode, which were counted using egrep (51).

To identify the ancestor strain that the isolated RSCVs evolved from, colony PCRs were performed using ancestor strain-specific primers. Forward primers contained the unique barcode used to tag each ancestor strain at the Tn7 site. Primers are indicated in Table S3.

To identify mutations, genomic DNA was isolated from colony variants using the DNeasy Blood and Tissue kit (Qiagen) according to the manufacturer's protocol. Clonal DNA was sequenced on the Illumina NextSeq 500 at the University of Pittsburgh Microbial Genomics Sequencing center using a modified protocol for library prep using the Illumina Nextera kit (52). 2x151bp sequencing reads for selected isolates were trimmed and quality filtered using Trimmomatic v0.36 (settings: LEADING:20 TRAILING:20 SLIDINGWINDOW:4:20 MINLEN:70) (53). The reads passing quality filtering were then used for variant calling with the open-source program *breseq* v0.30.0 using default settings (54).

Planktonic competition. To compete the six ancestor strains *in vitro*, strains were grown independently overnight in supplemented M9 medium (42.2 mM Na₂HPO₄, 22 mM KH₂PO₄, 21.7 mM NaCl, 18.7 mM NH₄Cl, 0.1 mM CaCl₂, 1 mM MgSO₄, and 11.1 mM glucose, supplemented with 20 ml/liter minimum essential medium [MEM] essential amino acids, 10 ml/liter MEM nonessential amino acids, and 1 ml each of trace mineral solutions A, B, and C [Corning catalog no. 25021-3Cl] [55]). Replicate tubes containing 5 ml supplemented M9 medium were inoculated with 50 μ l of each overnight culture. Each day, for 12 days (~80 generations total), 50 μ l of culture was transferred to a new tube filled with 5 ml supplemented M9 medium. Populations were frozen on days 1, 3, 4, 6, 7, 9, 10, and 12. At each time point, genomic DNA was isolated and sequenced as described above for mutation calling. Three replicates were sequenced at each time point. All sequencing reads from isolates are deposited in NCBI SRA under Biosample accession numbers [SAMN11956547](#) to [SAMN11956595](#).

c-di-GMP assays. c-di-GMP reporter plasmid pCdrA::gfp and empty vector pMH487 (31) were electroporated into selected isolates. Overnight cultures were diluted to an optical density at 600 nm (OD₆₀₀) of 0.1, and the cell pellets were resuspended in PBS. One hundred microliters were transferred to a polystyrene black 96-well plate (Corning). Cells were measured on a SpectraMax i3 plate reader (Molecular Devices) for OD₆₀₀ and GFP fluorescence. Fluorescence was measured as fluorescence intensity units (FIU) using an excitation of 485 nm and emission of 535 nm. Four biological replicates, each with three technical replicates, were performed. The FIU values were normalized to OD, and the average autofluorescence from the empty vector control was subtracted for each strain. The FIU of RSCVs was determined relative to the ancestor strain, which was set at 100%.

The *P. aeruginosa* PDE PA2133 was shuttled from pJN2133 (32) as an EcoRI-XbaI fragment into pHERD20T (56), forming the new plasmid pHERD2133. This was electroporated into selected isolates. Colony morphology was assayed on VBMM with 0.1% arabinose.

Biofilm assays. Microtiter crystal violet assays were performed as previously described (57). Briefly, overnight cultures were diluted 1:10 into fresh media, and 100 μ l was transferred into a 96-well round-bottom polyvinyl chloride (PVC) plate (Corning) and incubated for 24 h at 37°C in a humidified chamber. Biofilms were stained with 120 μ l of 0.1% crystal violet for 30 min at room temperature. Crystal violet was extracted with 150 μ l of 100% ethanol for 30 min at room temperature. One hundred microliters was transferred to a new plate, and OD₅₉₀ was measured on a SpectraMax i3 plate reader (Molecular Devices). Three biological replicates, each with two technical replicates, were performed.

Fitness assays. The ancestor strain PA14-1 was tagged with *lacZ* at the *attB* site to generate the strain PA14-1*attB*::*lacZ*. Briefly, miniCTX-*lacZ* (58) was conjugated into PA14-1. The vector backbone was removed by electroporating pFLP2 (59), which was subsequently cured by growth on LA supplemented with 10% sucrose. Colonies were screened for tetracycline and carbenicillin sensitivity and blue selection on 5-bromo-4-chloro-3-indolyl- β -D-galactopyranoside (X-Gal).

Overnight cultures were grown in 5 ml tryptic soy broth (TSB) (30 g/liter TSB). For each competition, five replicate tubes were inoculated with 25 μ l of overnight culture of both the RSCV and the marked ancestor (PA14-1*attB*::*lacZ*). Cultures were inoculated into tubes containing 5 ml of TSB either with a 7-mm polystyrene bead (biofilm) or without the bead (planktonic). After 24 h, 50 μ l of culture was transferred to a second tube containing fresh TSB for the planktonic cultures, and for the biofilm cultures, the biofilm-coated polystyrene bead was transferred to a second tube containing an uninoculated bead. After a second round of 24-h growth, all competitions were diluted and plated for CFU counts onto tryptic soy agar plates solidified with 1.5% agar and supplemented with 80 mg/ml X-Gal. In order to assess biofilm CFU, the beads were sonicated in PBS with a probe sonicator for 10 s at 30% power, and the resulting supernatant was used for plating. The selection coefficient (*s*) was calculated according to equation 1.

Prophage isolation and plaque assay. To isolate prophages from B23-2, an overnight culture of B23-2 was diluted 1:100 and incubated for 30 min at 37°C with shaking at 200 rpm. Mitomycin C (0.5 μ g/ml) was added to the culture, and the OD₆₀₀ was measured. The culture was reincubated, and the OD₆₀₀ was measured every hour. When the OD₆₀₀ began to decrease, the cells were pelleted by centrifugation, and the supernatant was filter sterilized and stored at 4°C.

To determine the level of susceptibility of *P. aeruginosa* strains to the bacteriophage(s) isolated from B23-2, 100 to 200 μ l of mid-log *P. aeruginosa* culture was incubated with 100- μ l serial dilutions of bacteriophage lysate for 15 min at 37°C. The infection was added to 5 ml molten soft agar (LB solidified with 0.7% agar) supplemented with 10 mM CaCl₂ and MgSO₄. This was then poured over solidified hard agar (LB solidified with 1.5% agar), allowed to solidify, and incubated overnight. The number of resulting plaques was then counted, and the number of PFU/ml was determined.

Statistical analysis. Data are presented as mean \pm standard deviation (SD). To determine whether data conformed to a normal distribution, a Shapiro-Wilk test was performed. All of the data sets were normally distributed except for the PFU/ml data (Fig. 6). For these data sets, means were compared using the nonparametric *t* test. All other comparisons were made using a one-way analysis of variance (ANOVA) with a Tukey's post-hoc test and Student's *t* test. Analyses were performed using GraphPad Prism v.5 (GraphPad Software). Statistical significance was determined using a *P* value of <0.05 .

Data availability. The reference sequences for variant calling were acquired from NCBI's RefSeq database (NC_002516.2 for PAO1, NC_008463.1 for PA14). All sequencing reads from isolates are deposited in NCBI SRA under Bioproject number PRJNA491911 and Biosample accession numbers SAMN10101410 to SAMN10101459.

SUPPLEMENTAL MATERIAL

Supplemental material for this article may be found at <https://doi.org/10.1128/mBio.01698-19>.

TEXT S1, PDF file, 0.2 MB.

FIG S1, PDF file, 0.1 MB.

FIG S2, PDF file, 0.4 MB.

FIG S3, PDF file, 0.3 MB.

FIG S4, PDF file, 1.6 MB.

FIG S5, PDF file, 2 MB.

FIG S6, PDF file, 0.4 MB.

TABLE S1, PDF file, 0.1 MB.

TABLE S2, PDF file, 0.01 MB.

TABLE S3, PDF file, 0.02 MB.

ACKNOWLEDGMENTS

We thank Michael Kann for his help with the planktonic and biofilm fitness assays.

A CFF Postdoctoral Research Fellowship (GLOAG17F0) supported E.S.G. V.S.C. and C.W.M. were supported by NIH grants (R01GM110444 and U01AI124302). D.J.W. was supported by NIH grants (R01AI077628, R01AI097511 and R01AI134895).

E.S.G. and C.W.M. performed the experimental work. J.S.H. performed the colony PCR. S.B.C. infected and sampled the porcine burn wounds. D.S. generated the sequence library. M.W. and G.R.L. quantified the strain frequency in the wounds. A.S.-L. and C.W.M. quantified the strain frequencies from planktonic growth. E.S.G., C.W.M., M.W., V.S.C., and D.J.W. conceptualized the project and wrote the manuscript.

REFERENCES

- Hall-Stoodley L, Costerton JW, Stoodley P. 2004. Bacterial biofilms: from the natural environment to infectious diseases. *Nat Rev Microbiol* 2:95–108. <https://doi.org/10.1038/nrmicro821>.
- Evans TJ. 2015. Small colony variants of *Pseudomonas aeruginosa* in chronic bacterial infection of the lung in cystic fibrosis. *Future Microbiol* 10:231–239. <https://doi.org/10.2217/fmb.14.107>.
- Lässig M, Mustonen V, Walczak AM. 2017. Predicting evolution. *Nat Ecol Evol* 1:0077. <https://doi.org/10.1038/s41559-017-0077>.
- Lind PA, Libby E, Herzog J, Rainey PB. 2019. Predicting mutational routes to new adaptive phenotypes. *Elife* 8:e38822. <https://doi.org/10.7554/eLife.38822>.
- Pesttrak MJ, Chaney SB, Eggleston HC, Dellos-Nolan S, Dixit S, Mathew-Steiner SS, Roy S, Parsek MR, Sen CK, Wozniak DJ. 2018. *Pseudomonas aeruginosa* rugose small-colony variants evade host clearance, are hyper-inflammatory, and persist in multiple host environments. *PLoS Pathog* 14:e1006842. <https://doi.org/10.1371/journal.ppat.1006842>.
- Haussler S, Tummler B, Weissbrodt H, Rohde M, Steinmetz I. 1999. Small-colony variants of *Pseudomonas aeruginosa* in cystic fibrosis. *Clin Infect Dis* 29:621–625. <https://doi.org/10.1086/598644>.
- Thomassen MJ, Demko CA, Boxerbaum B, Stern RC, Kuchenbrod PJ. 1979. Multiple isolates of *Pseudomonas aeruginosa* with differing antimicrobial susceptibility patterns from patients with cystic fibrosis. *J Infect Dis* 140:873–880. <https://doi.org/10.1093/infdis/140.6.873>.
- Boles BR, Thoendel M, Singh PK. 2004. Self-generated diversity produces “insurance effects” in biofilm communities. *Proc Natl Acad Sci U S A* 101:16630–16635. <https://doi.org/10.1073/pnas.0407460101>.
- Flynn KM, Dowell G, Johnson TM, Koestler BJ, Waters CM, Cooper VS. 2016. Evolution of ecological diversity in biofilms of *Pseudomonas aeruginosa* by altered cyclic diguanylate signaling. *J Bacteriol* 198:2608–2618. <https://doi.org/10.1128/jb.00048-16>.
- Hogardt M, Heesemann J. 2010. Adaptation of *Pseudomonas aeruginosa* during persistence in the cystic fibrosis lung. *Int J Med Microbiol* 300:557–562. <https://doi.org/10.1016/j.ijmm.2010.08.008>.
- Lam J, Chan R, Lam K, Costerton JW. 1980. Production of mucoid microcolonies by *Pseudomonas aeruginosa* within infected lungs in cystic fibrosis. *Infect Immun* 28:546–556.
- Singh PK, Schaefer AL, Parsek MR, Moninger TO, Welsh MJ, Greenberg EP. 2000. Quorum-sensing signals indicate that cystic fibrosis lungs are infected with bacterial biofilms. *Nature* 407:762–764. <https://doi.org/10.1038/35037627>.

13. Drenkard E, Ausubel FM. 2002. Pseudomonas biofilm formation and antibiotic resistance are linked to phenotypic variation. *Nature* 416: 740–743. <https://doi.org/10.1038/416740a>.
14. Kirisits MJ, Prost L, Starkey M, Parsek MR. 2005. Characterization of colony morphology variants isolated from *Pseudomonas aeruginosa* biofilms. *Appl Environ Microbiol* 71:4809–4821. <https://doi.org/10.1128/AEM.71.8.4809-4821.2005>.
15. Ma L, Jackson KD, Landry RM, Parsek MR, Wozniak DJ. 2006. Analysis of *Pseudomonas aeruginosa* conditional psl variants reveals roles for the psl polysaccharide in adhesion and maintaining biofilm structure postattachment. *J Bacteriol* 188:8213–8221. <https://doi.org/10.1128/JB.01202-06>.
16. Hengge R. 2009. Principles of c-di-GMP signalling in bacteria. *Nat Rev Microbiol* 7:263–273. <https://doi.org/10.1038/nrmicro2109>.
17. Starkey M, Hickman JH, Ma L, Zhang N, De Long S, Hinz A, Palacios S, Manoil C, Kirisits MJ, Starner TD, Wozniak DJ, Harwood CS, Parsek MR. 2009. *Pseudomonas aeruginosa* rugose small-colony variants have adaptations that likely promote persistence in the cystic fibrosis lung. *J Bacteriol* 191:3492–3503. <https://doi.org/10.1128/JB.00119-09>.
18. Pu M, Sheng L, Song S, Gong T, Wood TK. 2018. Serine hydroxymethyltransferase ShrA (PA2444) controls rugose small-colony variant formation in *Pseudomonas aeruginosa*. *Front Microbiol* 9:315. <https://doi.org/10.3389/fmicb.2018.00315>.
19. Goymer P, Kahn SG, Malone JG, Gehrig SM, Spiers AJ, Rainey PB. 2006. Adaptive divergence in experimental populations of *Pseudomonas fluorescens*. II. Role of the GGDEF regulator WspR in evolution and development of the wrinkly spreader phenotype. *Genetics* 173:515–526. <https://doi.org/10.1534/genetics.106.055863>.
20. Spiers AJ, Kahn SG, Bohannon J, Travisano M, Rainey PB. 2002. Adaptive divergence in experimental populations of *Pseudomonas fluorescens*. I. Genetic and phenotypic bases of wrinkly spreader fitness. *Genetics* 161:33–46.
21. Marvig RL, Sommer LM, Molin S, Johansen HK. 2015. Convergent evolution and adaptation of *Pseudomonas aeruginosa* within patients with cystic fibrosis. *Nat Genet* 47:57. <https://doi.org/10.1038/ng.3148>.
22. Smith EE, Buckley DG, Wu Z, Saenphimmachak C, Hoffman LR, D'Argenio DA, Miller SI, Ramsey BW, Speert DP, Moskowitz SM, Burns JL, Kaul R, Olson MV. 2006. Genetic adaptation by *Pseudomonas aeruginosa* to the airways of cystic fibrosis patients. *Proc Natl Acad Sci U S A* 103: 8487–8492. <https://doi.org/10.1073/pnas.0602138103>.
23. Roy S, Elgharably H, Sinha M, Ganesh K, Chaney S, Mann E, Miller C, Khanna S, Bergdall VK, Powell HM, Cook CH, Gordillo GM, Wozniak DJ, Sen CK. 2014. Mixed-species biofilm compromises wound healing by disrupting epidermal barrier function. *J Pathol* 233:331–343. <https://doi.org/10.1002/path.4360>.
24. Chaney SB, Ganesh K, Mathew-Steiner S, Stromberg P, Roy S, Sen CK, Wozniak DJ. 2017. Histopathological comparisons of *Staphylococcus aureus* and *Pseudomonas aeruginosa* experimental infected porcine burn wounds. *Wound Repair Regen* 25:541–549. <https://doi.org/10.1111/wrr.12527>.
25. Summerfield A, Meurens F, Ricklin ME. 2015. The immunology of the porcine skin and its value as a model for human skin. *Mol Immunol* 66:14–21. <https://doi.org/10.1016/j.molimm.2014.10.023>.
26. Sullivan TP, Eaglstein WH, Davis SC, Mertz P. 2001. The pig as a model for human wound healing. *Wound Repair Regen* 9:66–76. <https://doi.org/10.1046/j.1524-475x.2001.00066.x>.
27. Abdullahi A, Amini-Nik S, Jeschke MG. 2014. Animal models in burn research. *Cell Mol Life Sci* 71:3241–3255. <https://doi.org/10.1007/s00018-014-1612-5>.
28. Branda SS, Vik A, Friedman L, Kolter R. 2005. Biofilms: the matrix revisited. *Trends Microbiol* 13:20–26. <https://doi.org/10.1016/j.tim.2004.11.006>.
29. Haussler S, Fuqua C. 2013. Biofilms 2012: new discoveries and significant wrinkles in a dynamic field. *J Bacteriol* 195:2947–2958. <https://doi.org/10.1128/JB.00239-13>.
30. Friedman L, Kolter R. 2004. Two genetic loci produce distinct carbohydrate-rich structural components of the *Pseudomonas aeruginosa* biofilm matrix. *J Bacteriol* 186:4457–4465. <https://doi.org/10.1128/JB.186.14.4457-4465.2004>.
31. Rybtke MT, Borlee BR, Murakami K, Irie Y, Hentzer M, Nielsen TE, Givskov M, Parsek MR, Tolker-Nielsen T. 2012. Fluorescence-based reporter for gauging cyclic di-GMP levels in *Pseudomonas aeruginosa*. *Appl Environ Microbiol* 78:5060–5069. <https://doi.org/10.1128/AEM.00414-12>.
32. Hickman JW, Tifrea DF, Harwood CS. 2005. A chemosensory system that regulates biofilm formation through modulation of cyclic diguanylate levels. *Proc Natl Acad Sci U S A* 102:14422–14427. <https://doi.org/10.1073/pnas.0507170102>.
33. Poltak SR, Cooper VS. 2011. Ecological succession in long-term experimentally evolved biofilms produces synergistic communities. *ISME J* 5:369–378. <https://doi.org/10.1038/ismej.2010.136>.
34. Cady K, White A, Hammond J, Abendroth M, Karthikeyan R, Lalitha P, Zegans M, O'Toole G. 2011. Prevalence, conservation and functional analysis of *Yersinia* and *Escherichia* CRISPR regions in clinical *Pseudomonas aeruginosa* isolates. *Microbiology* 157:430–437. <https://doi.org/10.1099/mic.0.045732-0>.
35. Khan AI, Dinh DM, Schneider D, Lenski RE, Cooper TF. 2011. Negative epistasis between beneficial mutations in an evolving bacterial population. *Science* 332:1193–1196. <https://doi.org/10.1126/science.1203801>.
36. Cooper VS, Staples RK, Traverse CC, Ellis CN. 2014. Parallel evolution of small colony variants in *Burkholderia cenocepacia* biofilms. *Genomics* 104:447–452. <https://doi.org/10.1016/j.ygeno.2014.09.007>.
37. Rainey PB, Rainey K. 2003. Evolution of cooperation and conflict in experimental bacterial populations. *Nature* 425:72. <https://doi.org/10.1038/nature01906>.
38. Rainey PB, Travisano M. 1998. Adaptive radiation in a heterogeneous environment. *Nature* 394:69. <https://doi.org/10.1038/27900>.
39. Kim W, Levy SB, Foster KR. 2016. Rapid radiation in bacteria leads to a division of labour. *Nat Commun* 7:10508. <https://doi.org/10.1038/ncomms10508>.
40. Cady KC, Bondy-Denomy J, Heussler GE, Davidson AR, O'Toole GA. 2012. The CRISPR/Cas adaptive immune system of *Pseudomonas aeruginosa* mediates resistance to naturally occurring and engineered phages. *J Bacteriol* 194:5728–5738. <https://doi.org/10.1128/JB.01184-12>.
41. Ueda A, Wood TK. 2009. Connecting quorum sensing, c-di-GMP, pel polysaccharide, and biofilm formation in *Pseudomonas aeruginosa* through tyrosine phosphatase TpbA (PA3885). *PLoS Pathog* 5:e1000483. <https://doi.org/10.1371/journal.ppat.1000483>.
42. Malone JG, Jaeger T, Spangler C, Ritz D, Spang A, Arrieumerlou C, Kaever V, Landmann R, Jenal U. 2010. YfiB/NR mediates cyclic-di-GMP dependent small colony variant formation and persistence in *Pseudomonas aeruginosa*. *PLoS Pathog* 6:e1000804. <https://doi.org/10.1371/journal.ppat.1000804>.
43. Giddens SR, Jackson RW, Moon CD, Jacobs MA, Zhang XX, Gehrig SM, Rainey PB. 2007. Mutational activation of niche-specific genes provides insight into regulatory networks and bacterial function in a complex environment. *Proc Natl Acad Sci U S A* 104:18247–18252. <https://doi.org/10.1073/pnas.0706739104>.
44. Jones CJ, Newsom D, Kelly B, Irie Y, Jennings LK, Xu B, Limoli DH, Harrison JJ, Parsek MR, White P, Wozniak DJ. 2014. ChIP-Seq and RNA-Seq reveal an AmrZ-mediated mechanism for cyclic di-GMP synthesis and biofilm development by *Pseudomonas aeruginosa*. *PLoS Pathog* 10:e1003984. <https://doi.org/10.1371/journal.ppat.1003984>.
45. Irie Y, Starkey M, Edwards AN, Wozniak DJ, Romeo T, Parsek MR. 2010. *Pseudomonas aeruginosa* biofilm matrix polysaccharide Psl is regulated transcriptionally by RpoS and post-transcriptionally by RsmA. *Mol Microbiol* 78:158–172. <https://doi.org/10.1111/j.1365-2958.2010.07320.x>.
46. Gibson DG, Young L, Chuang R-Y, Venter JC, Hutchison CA, Smith HO. 2009. Enzymatic assembly of DNA molecules up to several hundred kilobases. *Nat Methods* 6:343–345. <https://doi.org/10.1038/nmeth.1318>.
47. Choi K-H, Schweizer HP. 2005. An improved method for rapid generation of unmarked *Pseudomonas aeruginosa* deletion mutants. *BMC Microbiol* 5:30. <https://doi.org/10.1186/1471-2180-5-30>.
48. Cooper VS. 2018. Experimental evolution as a high-throughput screen for genetic adaptations. *mSphere* 3:e00121-18. <https://doi.org/10.1128/mSphere.00121-18>.
49. Andrews S. 2010. FastQC: a quality control tool for high throughput sequencing data. Babraham Bioinformatics, Babraham Institute, Cambridge, United Kingdom.
50. Ewels P, Magnusson M, Lundin S, Käller M. 2016. MultiQC: summarize analysis results for multiple tools and samples in a single report. *Bioinformatics* 32:3047–3048. <https://doi.org/10.1093/bioinformatics/btw354>.
51. Martin M. 2011. Cutadapt removes adapter sequences from high-throughput sequencing reads. *Embnet J* 17:10–12. <https://doi.org/10.14806/ej.17.1-200>.
52. Baym M, Kryazhimskiy S, Lieberman TD, Chung H, Desai MM, Kishony R. 2015. Inexpensive multiplexed library preparation for megabase-sized genomes. *PLoS One* 10:e0128036. <https://doi.org/10.1371/journal.pone.0128036>.
53. Bolger AM, Lohse M, Usadel B. 2014. Trimmomatic: a flexible trimmer for

- Illumina sequence data. *Bioinformatics* 30:2114–2120. <https://doi.org/10.1093/bioinformatics/btu170>.
54. Deatherage DE, Barrick JE. 2014. Identification of mutations in laboratory-evolved microbes from next-generation sequencing data using breseq, p 165–188. *In* Sun L, Shou W (ed), *Engineering and analyzing multicellular systems: methods and protocols*. Springer, Berlin, Germany.
 55. Santos-Lopez A, Marshall CW, Scribner MR, Snyder D, Cooper VS. 2019. Biofilm-dependent evolutionary pathways to antibiotic resistance. *bioRxiv* <https://doi.org/10.1101/581611>.
 56. Qiu D, Damron FH, Mima T, Schweizer HP, Yu HD. 2008. PBAD-based shuttle vectors for functional analysis of toxic and highly regulated genes in *Pseudomonas* and *Burkholderia* spp. and other bacteria. *Appl Environ Microbiol* 74:7422–7426. <https://doi.org/10.1128/AEM.01369-08>.
 57. O'Toole GA. 2011. Microtiter dish biofilm formation assay. *J Vis Exp* 47:2437. <https://doi.org/10.3791/2437>.
 58. Hoang TT, Kutchma AJ, Becher A, Schweizer HP. 2000. Integration-proficient plasmids for *Pseudomonas aeruginosa*: site-specific integration and use for engineering of reporter and expression strains. *Plasmid* 43:59–72. <https://doi.org/10.1006/plas.1999.1441>.
 59. Hoang TT, Karkhoff-Schweizer RR, Kutchma AJ, Schweizer HP. 1998. A broad-host-range Flp-FRT recombination system for site-specific excision of chromosomally-located DNA sequences: application for isolation of unmarked *Pseudomonas aeruginosa* mutants. *Gene* 212:77–86. [https://doi.org/10.1016/s0378-1119\(98\)00130-9](https://doi.org/10.1016/s0378-1119(98)00130-9).
 60. Wolfgang MC, Kulasekara BR, Liang X, Boyd D, Wu K, Yang Q, Miyada CG, Lory S. 2003. Conservation of genome content and virulence determinants among clinical and environmental isolates of *Pseudomonas aeruginosa*. *Proc Natl Acad Sci U S A* 100:8484–8489. <https://doi.org/10.1073/pnas.0832438100>.